Recycling Iron-Containing Sludges from the Electroflocculation of Printing and Dyeing Wastewater into Anode Materials for Lithium-Ion Batteries

Gang Liu, Yiyao Shen, Peihua Ma, Sijia Zhao, Antoine Bonnefont, Yaokang Lv, Congze Wang, Laurent Ruhlmann, Cheng Zhang

Recycling Iron Containing Sludges from Electroflocculation of Printing and Dyeing Wastewater to Anode Materials for Li-ion Battery

Gang Liu,[a] Yiyao Shen,[a] Peihua Ma,[c] Sijia Zhao,[c] Antoine Bonnefont,[b], Yaokang Lv*[a], [b] Congze Wang,[a] Laurent Ruhlmann*[b] and Cheng Zhang*[a]

[a] G. Liu, Y. Shen, Dr. Y. Lv*, C. Wang, Dr. C. Zhang*
International Sci. & Tech. Cooperation Base of Energy Materials and Application, College of Chemical Engineering
Zhejiang University of Technology
Hangzhou 310014, P. R. China
E-mail: czhang@zjut.edu.cn; yaokanglv@zjut.edu.cn

[b] Dr. A. Bonnefont, Dr. Y. Lv*, Dr. L. Ruhlmann*
Institut de Chimie (UMR au CNRS n°7177)
Université de Strasbourg
4, rue Blaise Pascal CS 90032, F-67081 Strasbourg Cedex, France
E-mail: lruhlmann@unistra.fr

[c] P. Ma, S. Zhao
Shaoxing Jinye Environmental Protection Technology Co., Ltd.
No.173, Zhenghai Road, Binhai Industrial Zone, Keqiao District, Shaoxing, 312073, China.

Supporting information for this article is given via a link at the end of the document

Abstract: Fe-containing sludges DW/Fe were prepared by using electroflocculation treatment of printing and dyeing wastewater (DW) provided by a company. To further investigate the formation process and the properties of DW/Fe sludges and their application in anode materials of Li-ion battery, the DW/Fe sludges prepared from industrial wastewater were compared to three other sludges MB/Fe, RB/Fe, Ta/Fe prepared from model solutions containing either methyl blue (MB), rhodamine B (RB) or tartrazine (Ta). Also, DW/Fe sludges were calcined at 500 ℃ in N_2 atmosphere, to form iron oxide/carbon composite C-DW/Fe. The composition and structure of the sludges and of the C-DW/Fe composite were analyzed through FTIR, XRD, TGA, SEM, TEM and XPS, and their performances as anode of Li-ion batteries were studied by adding different proportions of conductive agent (super P® conductive carbon black). Our results show that the sludges are a complex of Fe_3O_4 and organic matter. The specific capacity and stability can be improved during the charge-discharge test by increasing the amount of carbon black. More importantly, this improvement is more pronounced on DW/Fe that does not require high temperature carbonization, which means sludges can not only protect the environment and avoid waste of resources, but also can be directly and widely used in decentralized energy storage devices.

Introduction

The wastewater discharged from printing and dyeing units has a great impact on the environment due to their high chemical oxygen demand (COD), low biochemical oxygen demand (BOD) and heavy colour.[1] In addition, some organic dyes may be toxic and carcinogenic to organisms.[2] Methods for treating dye wastewater generally include flocculation, coagulation[3], adsorption[4], reverse osmosis[5], foam separation[6] and chemical oxidation.[7] However, all these methods will produce large amounts of sludge products which may cause secondary pollution without further treatment.

Electroflocculation (EF) refers to the aggregation and sedimentation of particles in water or solution by electrochemical generation of a flocculant. The advantages of EF are mainly easy operation, lower quantities of produced sludge and reduction of the amount of chemicals.[8] The traditional methods of treating sludge are burning and burying, which can cause environmental pollution, the waste of resources and the increase of disposal costs.[9] In the recent years, a lot of new developments on sludge processing have been done. Anaerobic digestion (AD) can be a promising approach on energy recovery, sludge biodegradability, biogas composition and sludge stabilization, but it needs long payback times.[10] Bioelectrochemical systems (BES) are also unique technologies capable to convert the organic materials in sludge into useable forms of energy, such as electricity or hydrogen gas.[11] Interestingly, iron-containing sludge produced by EF can be used as electrode materials with a high proportion of transition metal oxides and/or metal hydroxides inside.[12] However, only few studies in this area have reported in detail the transformation of iron-containing sludge into electrode materials.

Transition metal oxides such as Co_3O_4, Fe_3O_4, Fe_2O_3 and MoO_3 and their composites have good Li-ion storage capacity due to the insertion/extraction of more than six Li-ion per formula unit.[13] As transition metal oxide, Fe_3O_4 has been highly investigated by researchers for its low cost, easy preparation and modification.[14] Especially when Fe_3O_4 fis combined with some carbon-based materials like Fe_3O_4/organic materials and Fe_3O_4/C, iimproved specific capacity and good stability can be achieved.[15-19]

In this present work, we used mixed dyeing wastewater collected from printing and dyeing companies as well as a variety of simulated printing and dyeing wastewaters containing either methyl blue (MB, Figure S1), tartrazine (Ta, Figure S2) or rhodamine B (RB, Figure S3) to prepare a large number of different sludges by EF named DW/Fe, MB/Fe, Ta/Fe and RB/Fe.

Due to the use of iron electrodes, these sludges contain a large amount of iron which can be directly used as anode electrode materials for Li-ion batteries. In order to study the performances of iron mud materials in batteries, DW/Fe was carbonized into C-DW/Fe in the atmosphere of N_2 at 500 ℃ to change the conductivity. The composition and morphology analysis of these materials were studied by FTIR, XRD, XPS, SEM and TEM. The performance of Li-ion battery anode materials made by adding super P® conductive carbon black in different proportions was analyzed by cyclic voltammetry (CV), electrochemical impedance spectroscopy (EIS) and charge and discharge tests. After the Li-

ion battery test, the second analysis of SEM, XRD and FTIR were performed once more on electrode materials. To summarize the properties of such materials, the addition of different proportions of super P® conductive carbon black to the electrodes had a great impact on the specific discharge capacity and stability of the sludge materials.

Results and Discussion

Morphological characterization

Schematic diagram of the formation process of the reddish-brown sludge nanomaterials, denoted DW/Fe is presented in Scheme 1. Similar preparation has been used for MB/Fe, RB/Fe, and Ta/Fe materials. In order to increase the carbon content and conductivity of the material after the EF process, the DW/Fe was calcinated at 500 °C in N_2 atmosphere for 2 hours to produce iron oxide/carbon composite denoted C-DW/Fe. EF is well adapted process for solutions containing dye molecules with anionic coloring groups (Figure S4). Figure 1a and Figure 1b show the SEM images of DW/Fe material, before the calcination process. The sludge is composed of agglomerated nanoparticles with a diameter between 100 and 200 nm. After calcination, the particles become less agglomerate and more independent due to the carbonization of organics (Figure 1c-1d). Energy dispersive spectroscopy (EDS) indicates that DW/Fe contains *ca.* 23% atom% Fe, 27% atom% C and 50% atom% O while C-DW/Fe contains *ca.* 24% atom% Fe, 36% atom% C and 40% atom% O (Figures S5-S6) indicating that the sludges contain large quantity of iron oxides mixed with carbon compounds. Figure 1e and Figure 1f show the TEM images of DW/Fe nanoparticles and suggest the presence of amorphous organic film on the surface of Fe_3O_4. The selected area diffraction pattern (red circle) of DW/Fe nanoparticles shows that they are crystalline. Furthermore, in Figure 1f, the distances between adjacent lattice planes are about 0.242 nm and 0.250 nm, which are in good agreement with the d-spacing of the (222) and (311) planes of Fe_3O_4 respectively. Figure 1g shows that C-DW/Fe has stronger diffraction spots than DW/Fe after calcination, and the calcination did not change the composition of the iron oxide corresponding to Fe_3O_4 as revealed by the d-spacing of (311) plane in Figure 1h.

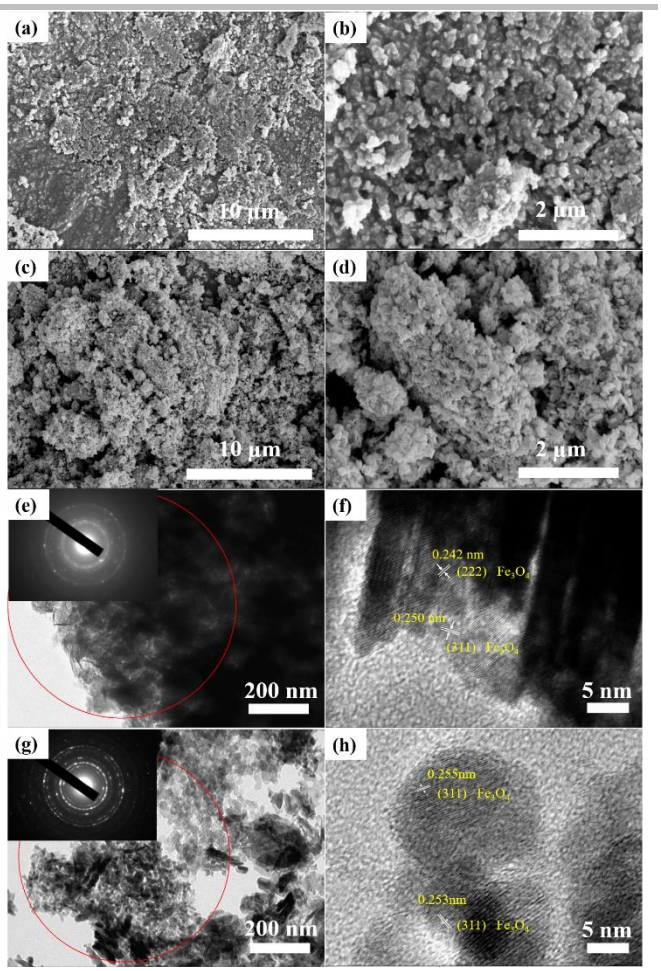

Figure 1. SEM images of DW/Fe sludge at (a) low magnification and (b) high magnification; SEM images of C-DW/Fe sludge at (c) low magnification and (d) high magnification. TEM images of the DW/Fe particles (e and f) and C-DW/Fe particles (g and h). The red circled area is the area selected for diffraction.

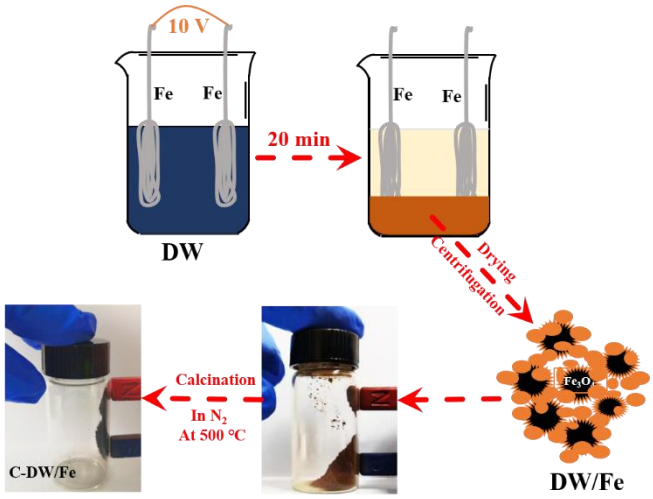

Scheme 1. Schematic diagram of the formation process of DW/Fe sludge nanomaterials and the preparation process of C-DW/Fe.

Powder X-ray diffraction (pXRD) spectra of composite materials of DW/Fe, MB/Fe, Ta/Fe, RB/Fe and C-DW/Fe are given in Figure 2a. They possess common diffraction peaks where the positions of these peaks match very well with the peak positions of Fe_3O_4 on the PDF card (PDF#19-0629). Nevertheless, the diffraction peaks of DW/Fe are significantly broader than the ones of MB/Fe, Ta/Fe and RB/Fe suggesting that the crystallinity of Fe_3O_4 in DW/Fe is lower than other materials. Additionally, some peaks at the 22 and 40 2θ-degree diffraction that do not belong to Fe_3O_4 appeared in the spectrum of DW/Fe and can be attributed to unknown compounds present in the wastewaters provided by the company. FT-IR spectra of DW/Fe and C-DW/Fe are displayed in Figure 2b. The absorption peaks of N-H, C-H, C-N, C=C, C-O and S=O at 3340 cm^{-1}, 2926 cm^{-1}, 1637 cm^{-1}, 1535 cm^{-1}, 1440 cm^{-1} and 1164 cm^{-1} respectively can be attributed to the small organic molecules belonging to the DW component.[20] This is confirmed by thermogravimetric (TGA) and differential thermal analysis (DTA) showing that DW/Fe, MB/Fe, Ta/Fe and RB/Fe sludges contain significant amount of organic dye molecules before the

calcination process (Figure S7). Interestingly, these peaks weakened and disappeared after calcination showing that the organic compound are carbonized and removed (Figure 2b).[21] Additionally, a very strong absorption peak was observed and occurred between 400 cm^{-1} and 800 cm^{-1} for DW/Fe, MB/Fe, RB/Fe, Ta/Fe and C-DW/Fe (Figures S8-S10), covering the fingerprint region absorption peak of some dye groups. This signal might be attributed to the iron oxide absorption peak.[22] Raman spectra were measured but were ill-defined except for MB/Fe and RB/Fe where the peaks could be better observed (Figure S11). For MB/Fe and RB/Fe, the peak positions of different dyes were nearly the same and coincide with the characteristic peaks of MB[23] and RB,[24] and no obvious band shift was observed.

For instance, in the case of MB/Fe (Figure S11), Raman spectrum fits well to the Raman spectrum of pure MB with four principal bands at 1193 cm^{-1}, 1386 cm^{-1}, 1529 cm^{-1} and 1619 cm^{-1}. The bands at 1193 cm^{-1}, 1386 cm^{-1} have been assigned to C-N stretching and the C-H in-plane ring deformation, respectively, while the two other bands at 1529 cm^{-1} and 1619 cm^{-1} were attributed to the C-C ring stretching for the MB dye. In the case of RB/Fe, the peak at 1193 cm^{-1} corresponds to C-H in-plane bend, while the peaks at 1355 cm^{-1}, 1503 cm^{-1} and 1645 cm^{-1} are due to stretching vibration of aromatic C-C bond.

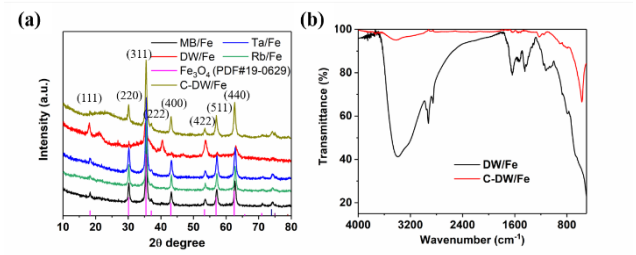

Figure 2. (a) XRD pattern of DW/Fe (red), MB/Fe (black), RB/Fe (green), Ta/Fe (blue) and C-DW/Fe (dark yellow); (b) FT-IR spectra of DW/Fe and of C-DW/Fe.

XPS analysis

X-ray photoelectron spectroscopy (XPS) was used to investigate the surface chemical composition of the sludges. The full XPS spectra of DW/Fe, MB/Fe, RB/Fe, Ta/Fe and C-DW/Fe are plotted in Figure 3a. The spectra reveal the presence of three main elements C, O and Fe in the sludges. The Fe content in the sludge is 22%-24% and obviously, the C content at the surface of C-DW/Fe increases a lot after the calcination as expected (Figure S12, Table S1). In Figure 3b, two peaks at 711.4 and 725.1 eV binding energies attributed to Fe $2p_{3/2}$ and Fe $2p_{1/2}$ respectively can be observed. Additionally, the Fe $2p_{3/2}$ peaks can be split into two peaks among the 710.9-711.1 (Fe(III)) and 713.2-713.4 (Fe(II)) with an area ratio approximately 5:3, which is very close to the 2:1 ratio expected for Fe_3O_4.[15,25] Based on the TEM and XPS analysis, the composites of sludges can be thought as Fe_3O_4 coated by organic matter. Note however, that the presence of the satellite peak at *ca.* 719 eV suggests that a small fraction of Fe_2O_3 which might exist on the surface of the particles.

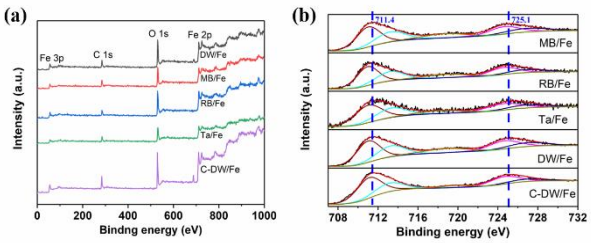

Figure 3. XPS spectra of DW/Fe, MB/Fe RB/Fe Ta/Fe and C-DW/Fe composites: (a) total scans; (b) Fe 2P (Fe $2p_{3/2}$ and Fe $2p_{1/2}$).

Cell performance

The anode electrodes of DW/Fe-8:1:1, C-DW/Fe-8:1:1, were prepared by coating the mixture containing 80 wt % iron-containing sludges, 10 wt % super P® conductive carbon black and 10 wt % PVDF binder on Cu foils while DW/Fe-5:4:1 and C-DW/Fe-5:4:1 were obtained by coating the mixture containing 50 wt % iron-containing sludges, 40 wt % super P® conductive carbon black and 10 wt % PVDF binder on Cu foils. Then, the anode electrodes were dried in vacuum oven at 60 °C for 12 hours. The electrochemical performance and lithium storage properties of anode electrodes were studied using galvanostatic charge/discharge experiments for 60 cycles at a current density of 100 $mA{\cdot}g^{-1}$ with a voltage window between 3.00 V and 0.05 V (*vs* Li/Li^+).

Analysis of CV performance

Typical cyclic voltammograms are represented in Figure 4 in the case of DW/Fe-8:1:1, DW/Fe-5:4:1, C-DW/Fe-8:1:1 and C-DW/Fe-5:4:1 respectively. For the first cathodic scan, three successive processes (peaks **1**, **2** and **7**) in Figure 4ab and two (peaks **1** and **2**) in Figure 4cd are observed representing first the reduction of Fe^{III} to Fe^{II} (Fe_3O_4 + x Li+ + x e- ⇄ $Li_x(Fe_3O_4)$), a quasi-reversible process observed at peak **1** for both DW/Fe-8:1:1 and DW/Fe-5:4:1) where Fe(III) are partially reduced, followed by two overlapping processes.[15-18] These additional processes (peak **2**) corresponded to the reduction of Fe^{III} and Fe^{II} ($Li_x(Fe_3O_4)$) to Fe^0,[16-19] as well as the formation of a solid electrolyte interface (SEI) layer (irreversible).[26-28]

It must be noted that the additional quasi-reversible wave (peak **7**) observed at 1.16 V in Figure 4ab does not occurred in second scan and is also inconspicuous or invisible in the case of MB/Fe, RB/Fe and Ta/Fe. It may be tentatively attributed to the organic components present in DW (Figures S13-S15).

Furthermore, during the first reverse anodic scan, a broad peak **3** between 1.0 and 2.5 V is observed for all samples and attributed to the oxidation of Fe^0 to Fe^{II} and to Fe^{III}.[15]

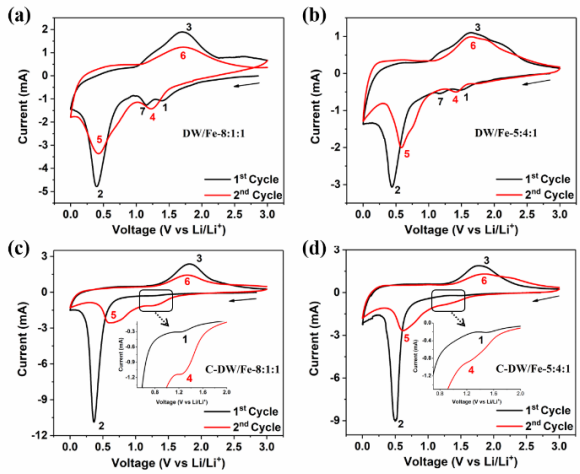

Figure 4. Cyclic voltammetry curves of DW/Fe-8:1:1 (a), DW/Fe-5:4:1 (b), C-DW/Fe-8:1:1 (c) and C-DW/Fe-5:4:1 (d). Scan rate: v = 1mV·s^{-1}.

In the second cathodic scan, two new peaks in reduction are observed (peaks **4** and **5)**. The peaks **2** measured at the first scan near 0.41 V decrease in intensity and shift to higher voltages while the peaks **1** near 1.45 V shift to more negative potential. The reason may be due to electrode polarization and a different type of $Li_xFe_3O_4$.[15] Another noteworthy phenomenon is that comparing with peaks **2**, the areas of the peaks **5** near 0.5 V is decreased a lot when the cycle number increased, indicating capacity loss caused by the irreversibility of the electrochemical reaction which may be attributed to the formation of SEI layer and the inactivation of iron materials. In the case of DW/Fe-5:4:1 sample, the first and the second reversed anodic scans (peaks **3** and **6**) are almost overlapped, and in case of C-DW/Fe-5:4:1, the areas of the peaks **3** and **6** in the first and the second anodic scans are close, indicating a good reversibility after the first cathodic scan. In contrast, a significant decrease of the anodic current is observed between the first and the second CV of the DW/Fe-8:1:1 and C-DW/Fe-8:1:1 samples revealing a decrease of the electrochemical performances upon potential scanning. In Figures S13-S15, the CV performance of the anode electrodes made for MB/Fe, RB/Fe and Ta/Fe are similar to DW/Fe. It indicated that the sludges produced by different dyes possess similar electrochemical properties, and the carbon black can protect the active materials from inactivation.

Charge-discharge behaviors of electrodes

The charge-discharge behaviors of DW/Fe and C-DW/Fe as the anode were thoroughly explored at 100 mA·g^{-1} between 0.05 V and 3.00 V and are displayed in Figure 5a-d. However, it must be noted that even if the ratio of DW/Fe and C-DW/Fe to carbon black is different, the electrodes prepared with the ratio of 8:1:1 and 5:4:1 show a similar first charge-discharge curves with a long voltage plateau at *ca.* 0.80 V attributed to the reduction of Fe^{III} to Fe^0. However, the first discharge capacity of DW/Fe-5:4:1 is 1777.5 mAh·g^{-1} significantly higher than of the one of DW/Fe-8:1:1 (1215.2 mAh·g^{-1}) and the theoretical specific capacity of pure Fe_3O_4 (924.0 mAh·g^{-1}).[16] Even after calcination, the first discharge capacity of C-DW/Fe-5:4:1 (1479.9 mAh·g^{-1}) is also higher than C-DW/Fe-8:1:1 (1200.6 mAh·g^{-1}) than Fe_3O_4. The high capacity of the first discharge process might be due to the formation of the SEI. The first discharge curves of DW/Fe are obviously not as smooth as C-DW/Fe for the presence of organic ingredients and this is also the reason for the higher specific capacity in first discharge process. Moreover, when the cycle number increased, the discharge capacities of DW/Fe-8:1:1 and C-DW/Fe-8:1:1 decreased rapidly and reached only 47.4 and 36.9 mAh·g^{-1} after 60 cycles, while the discharge capacity of DW/Fe-5:4:1 and C-DW/Fe-5:4:1 reached 690 mAh·g^{-1} and 223.6 mAh·g^{-1}, respectively, indicating that additional carbon black could stabilize the charge and discharge process of sludges and reduce the loss of specific capacity (Figures S16-S18). After the first cycle, the voltage of the plateau raises up from 0.8 to about 1.0 V due to the formation of an intermediate phase $Li_2Fe_3O_4$.[26]

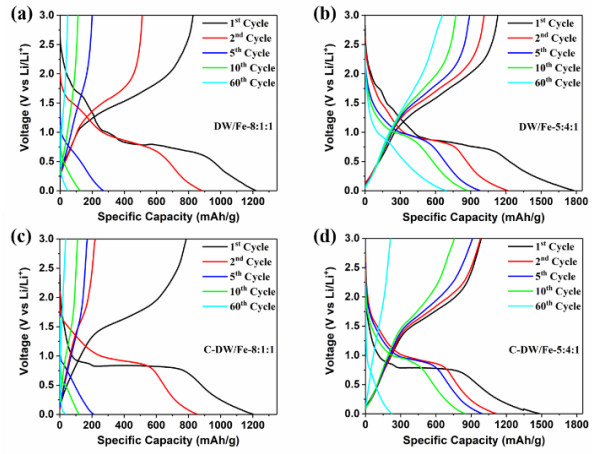

Figure 5. Galvanostatic charge-discharge curves of DW/Fe-8:1:1 (a), DW/Fe-5:4:1 (b), C-DW/Fe-8:1:1 (c) and C-DW/Fe-5:4:1 (d) at current density of 100 mA·g^{-1}.

Cycle performance of electrodes

The cycle performance of DW/Fe and C-DW/Fe at a current density of 100 mA·g^{-1} between 0.05 V and 3.00 V were shown in Figure 6a-d. It is obvious that the specific capacity for four electrodes decreases sharply in the first five cycles and the trend is getting flat for the electrodes with the ratio of 8:1:1 due to the very low capacity. For DW/Fe-5:4:1, the capacity becomes stable after 10 cycles, while the electrode of C-DW/Fe-5:4:1 is decreasing fast during the first 30 cycles. Moreover, the capacity of DW/Fe-5:4:1 is 3 times higher than C-DW/Fe-5:4:1 at the 60th cycle indicating that carbon black is more suitable for non-calcinated DW/Fe. In addition, the first coulombic efficiency of all electrodes is below 70%. Nevertheless, the coulombic efficiency of DW/Fe-5:4:1 and C-DW/Fe-5:4:1 rises up to 83.6% and 88.01 % respectively at the second cycle and exceeds 90.0% after the fourth cycle, while for DW/Fe-8:1:1 and C-DW/Fe-8:1:1 the coulombic efficiency is less than 80% before the 7th and 5th cycle, respectively, where a significant decline occurred in second charge-discharge progress resulting in a final capacity shortage. These phenomena also appear in the other three sludges (Figures S19-S21) proving that more carbon black can improve the efficiency of electrodes.

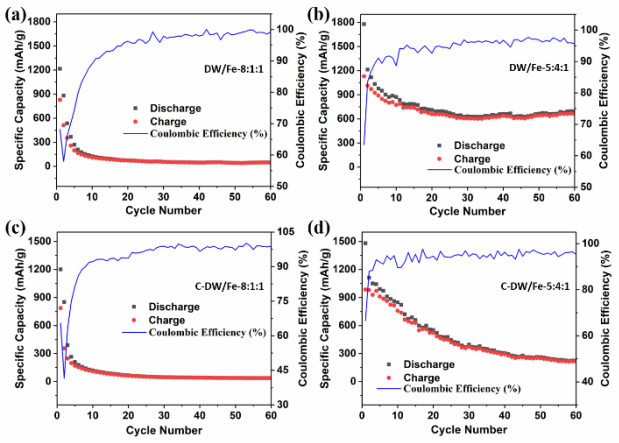

Figure 6. Cycling stability of DW/Fe-8:1:1 (a), DW/Fe-5:4:1 (b), C-DW/Fe-8:1:1 (c) and C-DW/Fe-5:4:1 (d) at a current density of 100 mA·g^{-1} between 0.05 V and 3.00 V.

Rate capability of electrodes

Rate capability of the sludge electrodes were shown in Figure 7. With the current density increasing from 50 to 400 mA·g^{-1} a descending ladder can be found though the capacity changed a lot in first 20 cycles. Comparing with Figure 6b, the capacity of DW/Fe-5:4:1 (690 ± 60 mAh·g^{-1}) between 11 and 20 cycle in Figure 7 is very close to 760 (± 60) mAh·g^{-1}. Even at high current density of 200 mA·g^{-1}, 300 mA·g^{-1} and 400 mA·g^{-1}, the DW/Fe-5:4:1 electrode can still give a high average capacity of 550 mAh·g^{-1}, 460 mAh·g^{-1} and 445 mAh·g^{-1}, respectively, which are higher than the theoretical specific capacity of the widely used graphite anode material (372 mAh·g^{-1}).[18] The most important result is that the capacity of DW/Fe-5:4:1 can keep 620 (± 10) mAh·g^{-1} when the current density returns to 50 mA·g^{-1}, indicating good-rate for DW/Fe-5:4:1 electrode. In addition, the electrodes of RB/Fe-5:4:1, MB/Fe-5:4:1 and Ta/Fe-5:4:1 also show good recovery when the current density changes from 400 to 50 mA·g^{-1}.

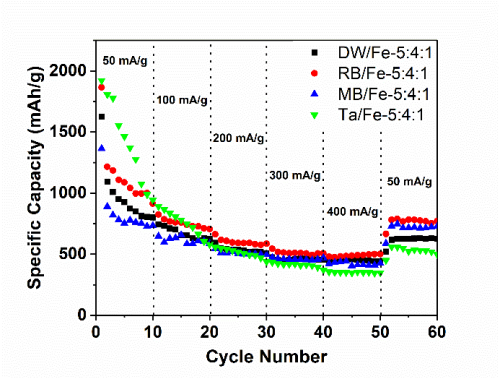

Figure 7. Rate capability of DW/Fe-5:4:1 (black), RB/Fe-5:4:1 (red), MB/Fe-5:4:1 (blue) and Ta/Fe-5:4:1 (green) electrodes at various current density between 50 and 400 mA·g^{-1}.

Analysis and simulation calculation of EIS

In order to understand the influence of the carbon black addition and of the calcination on the electrochemical properties, electrochemical impedance spectroscopy (EIS) measurements were performed after the CV tests. The impedance spectra were fitted by the equivalent circuit displayed in Figure 8b, taking into account the electrolyte, the SEI, and the charge transfer resistances, R_s, R_{SEI}, R_{ct}, respectively, the constant phase element CPE_1 and CPE_2, the lithium intercalation capacitance C_{int}, and the Warburg impedance associated to lithium diffusion Z_w.[28]

The Nyquist plots of MB/Fe, RB/Fe and Ta/Fe were given in Figure S22 while the Nyquist plots of DW/Fe-5:4:1, C-DW/Fe-8:1:1 and C-DW/Fe-5:4:1 were displayed in Figure 8a. By fitting the impedance spectra, the intercalation capacitances could be estimated to 6200 and 7400 µF for C-DW/Fe-8:1:1 and C-DW/Fe-5:4:1 respectively. In the case of C-DW/Fe-8:1:1 and C-DW/Fe-5:4:1 samples, only a single semi-circle is observed in the intermediate frequency range, which can be attributed to the SEI resistance coupled to the SEI film capacitance.[18] Interestingly, the impedance spectra of the non-calcinated sample DW/Fe-5:4:1 displays three arcs, with two semi-circles in the middle frequency range and the intercalation capacitance arc at low frequencies. One of the semi-circles at low frequency is due to the SEI film, while the appearance of the second semi-circle can be attributed to the charge transfer resistance and to the decrease of the electronic conductivity of the non-calcinated electrode materials compared to the calcinated one. A decrease of R_{SEI} (from *ca.* 200 Ω for C-DW/Fe-8:1:1 and C-DW/Fe-5:4:1 to 145 Ω for DW/Fe-5:4:1) is observed (Table S2). In addition, the intercalation capacitance increases by a factor of approximately 2 to *ca.* 14000 µF compared with the calcinated samples. The decrease of R_{SEI} and the increase of C_{int} might be attributed to the smaller size of the Fe_3O_4 particles in the non-calcinated samples (Table S3). The size of Fe_3O_4 crystallites in DW/Fe is smaller than C-DW/Fe which can explain the decrease the R_{SEI} and also the improved performance of the material. The results are in qualitative agreement with the values determined by the charge/discharge cycles.

We observed that C-DW/Fe has a poorer Li-ion battery performance than DW/Fe. C-DW/Fe and DW/Fe. Unlike the first discharge curves of C-DW/Fe, DW/Fe possesses many small steps which can be attributed to the existence of organic group from dyes, and the organic groups probably have a certain capacity through its own redox reaction which will be enhanced the performance of DW/Fe. Then, the Fe_3O_4 particles surrounded by dyes have low mechanical strength, which maybe helps the lattice not to be destroyed during the insertion and extraction of Li-ion. In the future, the influence of the presence of heteroatom in the materials will be investigated in more details.

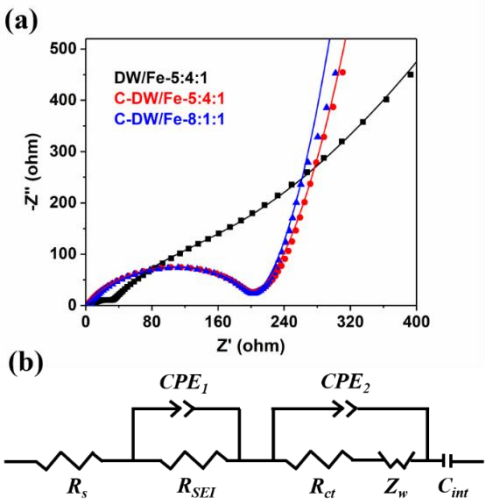

Figure 8. (a) Nyquist plots of DW/Fe-5:4:1, C-DW/Fe-8:1:1 and C-DW/Fe-5:4:1 tested in the Li-ion battery with open circuit voltage after the CV test. (b) Equivalent circuit.

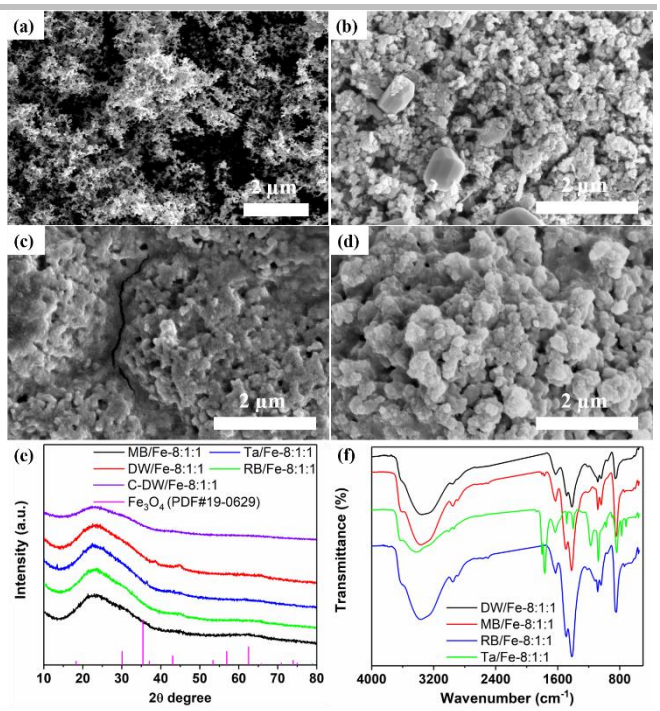

Figure 9. SEM image of (a) super P® conductive carbon black, (b) DW/Fe-8:1:1 after being coated on copper foil, (c) DW/Fe-8:1:1 coated on copper foil after 60 cycles of charge and discharge test, (d) DW/Fe-5:4:1 coated on copper foil after 60 cycles of charge and discharge test; (e) pXRD pattern of DW/Fe-8:1:1, C-DW/Fe-8:1:1, MB/Fe-8:1:1, RB/Fe-8:1:1 and Ta/Fe-8:1:1 scraping from copper foil after 60 cycles of charge and discharge test; (f) FT-IR spectra of DW/Fe-8:1:1, MB/Fe-8:1:1, RB/Fe-8:1:1 and Ta/Fe-8:1:1 after 60 cycles of charge and discharge test.

Analysis of electrode materials after battery test

To further study the changes in DW/Fe-8:1:1 with a small amount of black carbon during the cell testing, SEM test was used to characterize the materials and explain the rapid decline in battery performance. As shown in Figure 9a, super P® conductive carbon black is a loose, small and uniform particles. After mixing super P and DW/Fe, the particles of DW/Fe-8:1:1 coated on copper foil (Figure 9b) become more loosely compared with Figure 1b, which can be attributed to the wrapping by the carbon black. But after 60 cycles of charge and discharge, uniformly dispersed particles are replaced by a tight packing with sags and cracks (see Figure 9c). Unlike to DW/Fe-8:1:1, the electrode of DW/Fe-5:4:1 after 60 cycles of charge and discharge test seems to maintain good graininess (Figure 9d). In addition, EDS analysis shows that the atomic percentage of elemental Fe has dropped by more than 50% after the cell performance testing (Figures S23-S25, Table S4). In order to further study structural changes, the pXRD pattern and IR spectra of DW/Fe-8:1:1, C-DW/Fe-8:1:1, MB/Fe-8:1:1, RB/Fe-8:1:1 and Ta/Fe-8:1:1 are given in Figure 9e and Figure 9f respectively. The broad peak at 2θ=25° can be attributed to the presence of non-crystalline carbon. It can be noted that the diffraction peaks and the absorption peak corresponding to Fe_3O_4 disappeared. One possible explanation may be that the crystal form of Fe_3O_4 was destroyed due to unequal intercalation and deintercalation behaviors of Li^+ in the crystal lattice. Finally, it should be noticed that after 60 cycles of charge and discharge, the IR spectra (Figure 9f and Figures S8-S10) are significantly modified, indicating that the dyes are decomposed under charge-discharge cycling. However, even if the dye molecules are decomposed, some functional groups (like C-N, evidenced by a peak at 1637 cm^{-1} in the IR spectrum in Figure 9f) and chemical elements (such as Sulfur, evidenced in EDS spectra) stemming from the dyes can still be detected in the materials.

Conclusion

In this work, we used electroflocculation to treat the wastewater from company and investigated the possibility to use the obtained Fe-containing sludges in Li-ion batteries. We compared the properties of the sludges with the ones obtained by simulated wastewater containing iron and dyes such as Methylene Blue, Rhodamine B and Tartraazine. After addition of carbon black, the Li intercalation/deintercalation performance was investigated. The sludges have higher specific capacity in first discharge than the theoretical specific capacity of Fe_3O_4. However, the specific capacity drops when the amount of carbon black is reduced. The reasons can be attributed to the follow: *i)* Higher amount of carbon black increases the conductivity of the electrode, which facilitates the intercalation and deintercalation of lithium ions and reduces the loss of specific capacity. *ii)* Increased carbon black fraction can effectively prevent the agglomeration of iron oxide nano-particles during the charge and discharge progress, reduce the polarization of sludges and thus stabilize the specific capacity.

In summary, we have shown that wastewater from companies can be recycled to produce Fe-containing sludges which can be used in the field of energy storage. This allows the enterprises not only to save money (around 428 $ per tonne, 384 € per tonne or 3000 RMB per tonne of wastewater treatment and operation cost), but also to recycle waste that could be harmful to the environment. Additionally, there is a gap between the performance of sludges and the performance of many already reported Fe_3O_4 materials (see Table S5). The addition of conductive binder such as carbon black can effectively improve the energy storage performance of

Fe-containing sludges which can be used as a low cost and abundant source of iron oxide.

Experimental Section

Materials

All chemicals used in this article were commercially available, unless otherwise specified. Sodium sulfate (Na_2SO_4), methyl blue (MB, $C_{37}H_{27}N_3Na_2O_9S_3$), tartrazine (Ta, $C_{16}H_9N_4O_9S_2Na_3$) and rhodamine B (RB, $C_{28}H_{31}ClN_2O_3$) were purchased from Aladdin. Super P® conductive carbon black (C), Poly(vinylidene fluoride) (PVDF) and N-Methyl pyrrolidone (NMP) were obtained from the Shanxi Lizhiyuan Battery Material Co., Ltd. (Taiyuan China). Dyeing wastewater (DW) was collected from Zhejiang Dongsheng Printing and Dyeing Co., Ltd. (Shaoxing, China) in a multi-dye mixed waste tank. The iron wire was purchased from hardware store. All reagents were used as received without further purification.

Preparation of DW/Fe, MB/Fe, RB/Fe, Ta/Fe and C-DW/Fe composites

These composites were prepared by EF applying a DC voltage of 10 V in a 0.35 mol·L^{-1} aqueous solution of Na_2SO_4 for 20 min. The concentrations of dyes MB, RB, Ta were 1.875 mmol·L^{-1}. The concentration and composition of DW obtained from company was more complicated to be determinate, but the total chemical oxygen demand (COD) of DW was 2300 g·L^{-1}. Iron wires (Φ=2.8 mm) with a ring shape were used for cathode and anode. The suspension obtained by electro-sedimentation was separated by centrifugation at a speed of 4000 rpm for 5 min, and then these complexes were washed 3 times with deionized water to remove residual electrolyte before being placed in a drying oven at 60 °C for 6 hours. Finally, these materials were transferred to a vacuum oven and dried at 60 °C for 12 hours.

C-DW/Fe were made by calcining the DW/Fe in N_2 atmosphere at 500 °C for 2 hours. Before the calcination, DW/Fe was placed in a tube furnace with a N_2 flow rate of 100 mL·min^{-1} for 2 hours and the heating rate is 3 °C·min^{-1}.

Characterization

Infrared (IR) spectra were adopted using a Nicolet 6700 spectrometer (Thermo Fisher Nicolet, USA) with KBr pellets. Raman spectra were recorded on LabRam HR UV 800 Raman Spectrometer (Jobin Yvon, France) at 632.81 nm. UV-vis spectra were obtained using a UV-1800 spectrophotometer (Shimadzu, Japan), and visible and NIR transmission spectra was performed in 0.035 mol·L^{-1} Na_2SO_4 solution. Powder X-ray diffraction (PXRD) experiments were performed using a X'Pert Pro diffractometer with Cu-Kα radiation (λ= 1.5418Å) operating at 40 kV and 40 mA and the scanning angle ranged from 10° to 80° of 2θ. Scanning electron microscopy (SEM) images were collected using a field emission scanning electron microscope (Zeiss Gemini 300). Transmission Electron Microscope (TEM) images were obtained from a JEOL JEM 2100. Thermogravimetric analyses (TGA) were performed on a Q5000IR (Ra, USA) thermogravimetric analyzer running from room temperature to 1000 °C at a heating rate of 10 °C·min^{-1} in nitrogen. X-ray photoelectron spectra (XPS) were operated on a spectrometer (Kratos AXIS Ultra DLD, Shimadzu, Japan).

Electrochemical measurements

The anode electrodes of DW/Fe-8:1:1, MB/Fe-8:1:1, RB/Fe-8:1:1, Ta/Fe-8:1:1 and C-DW/Fe-8:1:1 were prepared by coating the mixture containing 80 wt % iron-containing sludges, 10 wt% super P® conductive carbon black and 10 wt % PVDF binder on Cu foils. The other anodes DW/Fe-5:4:1 MB/Fe-5:4:1, RB/Fe-5:4:1, Ta/Fe-5:4:1 and C-DW/Fe-5:4:1 were prepared by coating the mixture containing 50 wt % iron-containing sludges, 40 wt % super P® conductive carbon black and 10 wt % PVDF binder on Cu foils. All the electrodes coated on Cu foils were dried in vacuum oven at 60 °C for 12 hours before being cut into circular Cu current collector foils. The cell assembled with the lithium foil as the cathode, the circular electrode as the anode, and 1 mol·L^{-1} $LiPF_6$ dissolved in ethylene carbonate (EC), dimethyl carbonate (DMC) and diethyl carbonate (DEC) (EC:DMC:DEC=1:1:1) as the electrolyte in glove-box filled with Ar using CR2032 casing. The charge-discharge measurements of cells were carried out on LAND CT2001A in the voltage range of 0.05 -3.00 V *vs* Li/Li$^+$ using a constant current density at room temperature. Electrochemical Impedance Spectroscopy (EIS) experiments were carried out at open circuit voltage (OCV, around 2.5 V) in the frequency range from 0.01 Hz – 0.10 MHz in CHI 660E electrochemical working station using the assembled Li-ion half-cells.

Acknowledgements

We sincerely thank the support from Zhejiang Provincial Natural Science Foundation of China (No. LY19B010003, LZ17E030001) and National Natural Science Foundation of China (NSFC, No. 21501148, 51673174). LR and AB also thank the Université de Strasbourg for the projet "Idex Attractivité 2012" as well as the Labex CSC (Chemistry of Complex Systems) which has also supported one part of this research.

Keywords: Fe-containing sludges • Electroflocculation • Wastewater • Anode materials of Li-ion battery • Fe_3O_4

[1] a) X. Hu, L. Lei, G. Chen, P. Yue, *Water Res.* **2001**, *35*, 2078-2080; b) P. Sun, L. Xu, J. Li, P. Zhai, H. Zhang, Z. Zhang, W. Zhu, *Chem. Eng. J.* **2018**, *334*, 377-388; c) A. K. Verma, R. R. Dash, P. Bhunia, *J. Environ. Manag.* **2012**, *93*, 154-168.

[2] a) P. Luo, Y. Zhao, B. Zhang, J. Liu, Y. Yang, J. Liu, *Water Res.* **2010**, *44*, 1489-1497; b) S. Mei, J. Gu, T. Ma, X. Li, Y. Hu, W. Li, J. Zhang, Y. Han, *Chem. Eng. J.* **2019**, *371*, 118-129.

[3] a) F. El-Gohary, A. Tawfik, *Desalination* **2009**, *249*, 1159-1164; b) V. Golob, A. Vinder, M. Simoni, *Dyes Pigm.* **2005**, *67*, 93-97.

[4] S. Karcher, A. Kornmüller, M. Jekel, *Water Res.* **2002**, *36*, 4717-4724.

[5] N. Al-Bastaki, *Chem. Eng. Proc.* **2004**, *43*, 1561-1567.

[6] K. Lu, X. Zhang, Y. Zhao, Z. Wu, *J. Hazard. Mater.* **2010**, *182*, 928-932.

[7] a) S. Kang, H. Chang, *Water Sci. Technol.* **1997**, *36*, 215-222; b) M. Pérez, F. Torrades, X. Domènech, *J. Peral, Water Res.* **2002**, *36*, 2703-2710.

[8] a) B. Khaled, B. Wided, H. Soumaya, E. Elimame, L. Mouna, H. Béchir, *J. Hazard. Mater.* **2018**, *344*, 968-980; b) M. R. D. C. Marques, P. S. A. D. Souza, M. M. Rigo, A. A. Cerqueira, J. L. D. Paiva, F. Merçon, D. V. Perez, *Environ. Sci. Pollut. Res. Int.* **2015**, *22*, 15985-15993; c) J. P. P. B. Rech, A. T. Paulino, *Clean Techn. Environ. Policy* **2019**, *21*, 1155-1163; d) T. Harif, A. Adin, *Water Res.* **2011**, *45*, 6195-6206.

[9] a) J. R. Beegle, A. P. Borole, *Environ. Sci. Water Res. Technol.* **2017**, *3*, 1073-1085; b) S. T. Oh, J. R. Kim, G. C. Premier, T. H. Lee, C. Kim, W. T. Sloan, *Biotechnol. Adv.* **2010**, *28*, 871-881.

[10] a) H. Carrère, C. Dumas, A. Battimelli, D. J. Batstone, J. P. Delgenès, J. P. Steyer, I. Ferrer, *J. Hazard. Mater.* **2010**, *183*, 1-15; b) A. N. Kumar, A. K. Bandarapu, S. V. Mohan, *Chem. Eng. J.* **2019**, *374*, 1264-1274; c) V. Penaud, J. P. Delgenès, R. Moletta, *Enzyme Microb. Technol.* **1999**, *25*, 258-263; d) B. Yu, J. B. Xu, H. P. Yuan, Z. Y. Lou, J. X. Lin, N. W. Zhu, *Fuel* **2014**, *130*, 279-285.

[11] a) B. E. Logan, B. Hamelers, R. Rozendal, U. Schröder, J. Keller, S. Freguia, P. Aelterman, W. Verstraete, K. Rabaey, *Environ. Sci. Technol.* **2006**, *40*, 5181-5192; b) R. A. Rozendal, H. V. M. Hamelers, K. Rabaey, J. Keller, C. J. N. Buisman, *Trends Biotechnol.* **2008**, *26*, 450-459; c) H. Liu, S. Grot, B. E. Logan, *Environ, Sci. Technol.* **2005**, *39*, 4317-4320.

[12] a) Z. Wu, H. Yue, L. Li, B. Jiang, X. Wu, P. Wang, *J. Power Sources* **2010**, *195*, 2888- 2893; b) H. Kang, G. Wang, H. Guo, M. Chen, C. Luo, K. Yan, *Ind. Eng. Chem. Res.* **2012**, *51*, 7923-7931.

[13] a) R. Wu, X. Qian, K. Zhou, J. Wei, J. Lou, P. M. Ajayan, *ACS Nano* **2014**, *8*, 6297-6303; b) R. Wu, X. Qian, X. Rui, H. Liu, B. Yadian, K. Zhou, J. Wei, Q. Yan, X.-Q. Feng, Y. Long, L. Wang, Y. Huang, *Small* **2014**, *10*,

1932-1938; c) C. Ban, Z. Wu, D. T. Gillaspie, L. Chen, Y. Yan, J. L. Blackburn, A. C. Dillon, Adv. Mater. 2010, 22, E145-E149; d) Y.-S. Hu, Y.-G. Guo, W. Sigle, S. Hore, P. Balaya, J. Maier, *Nat. Mater.* **2006**, *5*, 713-717; e) P. Balaya, H. Li, L. Kienle, J. Maier, *Adv. Funct. Mater.* **2003**, *13*, 621-625.

[14] a) R. Wu, X. Qian, K. Zhou, J. Wei, J. Lou, P. M. Ajayan, *ACS Nano* **2014**, *8*, 6297-6303; b) R. Wu, X. Qian, X. Rui, H. Liu, B. Yadian, K. Zhou, J. Wei, Q. Yan, X.-Q. Feng, Y. Long, L. Wang, Y. Huang, *Small* **2014**, *10*, 1932-1938; c) C. Ban, Z. Wu, D. T. Gillaspie, L. Chen, Y. Yan, J. L. Blackburn, A. C. Dillon, Adv. Mater. 2010, 22, E145-E149; d) Y.-S. Hu, Y.-G. Guo, W. Sigle, S. Hore, P. Balaya, J. Maier, *Nat. Mater.* **2006**, *5*, 713-717; e) P. Balaya, H. Li, L. Kienle, J. Maier, *Adv. Funct. Mater.* **2003**, *13*, 621-625.

[15] T. Yoon, C. Chae, Y. K. Sun, X. Zhao, H. K. Harold, J. K. Lee, *J. Mater. Chem.* **2011**, *21*, 17325.

[16] L. Chun, X. Wu, X. Lou, Y. Zhang, *Electrochim. Acta* **2010**, *55*, 3089-3092.

[17] S. Jin, H. Deng, D. Long, X. Liu, L. Zhan, X. Liang, W. Qiao, L. Ling, *J. Power Sources* **2011**, *196*, 3887-3893.

[18] C. Yan, C. Wu, Q. Zhuang, L. Tian, Y. Cui, X. Zhao, Z. Ju, X. Sun, *ChemistrySelect* **2016**, *1*, 3979-3991.

[19] a) P. Lian, X. Zhu, H. Xiang, Z. Li, W. Yang, H. Wang, *Electrochim. Acta* **2010**, *56*, 834-840; b) Y. He, L. Huang, J. Cai, X. Zheng, S. Sun, *Electrochim. Acta* **2011**, *55*, 1140-1144.

[20] a) A. Lin, S. Shao, H. Li, D. Yang, Y. Kong, *J. Membr. Sci.* **2011**, *371*, 286–292; b) N. M. Shishlov, Sh. S. Akhmetzyanov, S. L. Khursan, Russ. *J. Phy. Chem. B.* **2010**, *4*, 846-859; c) D. Xue, D. Zhu, H. Duan, Z. Wang, Y. Lv, W. Xiong, L. Li, M. Liu, L. Gan, *Chem. Commun.* **2019**, *55*, 11219–11222.

[21] a) Z. Song, H. Duan, D. Zhu, Y. Lv, W. Xiong, T. Cao, L. Li, M. Liu, L. Gan, *J. Mater. Chem. A*, **2019**, *7*, 15801–15811; b) L. Miao, H. Duan, Z. Wang, Y. Lv, W. Xiong, D. Zhu, L. Gan, L. Li, M. Liu, *Chem. Eng. J.* **2020**, *382*, 122945; c) X. Qian, L. Miao, J. Jiang, G. Ping, W. Xiong, Y. Lv, Y. Liu, L. Gan, D. Zhu, M. Liu, *Chem. Eng. J.* **2020**, *388*, 124208.

[22] a) M. Kumari, U. Charles, Jr. Pittman, D. Mohan, *J. Colloid Interface Sci.* **2015**, *442*, 120-132; b) J. Jaber, E. Mohsen, *Mater. Res. Bull.* **2016**, *73*, 409-422; c) C. Zhang, Z. Mo, R. Guo, G. Teng, G. Zhao, *Mater. Res. Bull.* **2014**, *53*, 116-112.

[23] E. B. Santos, E. C. N. L. Lima, C. S. Oliveira, F. A. Sigoli, I. O. Mazali, *Anal. Methods*, **2014**, *6*, 3564-3568.

[24] X. H. Zu, Z. H. Jian, G. B. Yi, H. L. Huang, B. B. Zhong, H. S. Luo, J. R. Huang, C. Wang, *Chin. J. Polym. Sci.* **2015**, *33*, 1470–1476.

[25] a) H. Guo, H. Wang, N. Zhang, J. Li, J. Liu, A. Alsaedi, T. Hayat, Y. Li, Y. Sun, *Chem. Eng. J.* **2019**, *369*, 736-744; b) Y. Zhao, R. Zhang, H. Liu, M. Li, T. Chen, D. Chen, X. Zou, L. F. Ray, *Chem. Eng. J.* **2019**, *375*, 122011; c) W. Wang, J. Si, J. Li, Q. Wang, S. Chen, *Int. J. Hydrogen Energy* **2016**, *41*, 16858-16864.

[26] a) P. Poizot, S. Laruelle, S. Grugeon, L. Dupont, J. Tarascon, *Nature* **2000**, *407*, 496-499; b) Y. Chen, L. He, P. Shang, Q. Tang, Z. Liu, H. Liu, L. Zhou, *J. Mater. Sci. Technol.* **2011**, *27*, 41-45.

[27] Y. Piao, H. S. Kim, Y. Sung, T. Hyeon, *Chem. Commun.* **2010**, *46*, 118-120.

[28] L. Li, A. Kovalchuk, H. Fei, Z. Peng, Y. Li, N. D. Kim, C. Xiang, Y. Yang, G. Ruan, J. M. Tour, *Adv. Energy Mater.* **2015**, *5*, 1500171.

Entry for the Table of Contents

Insert graphic for Table of Contents here.

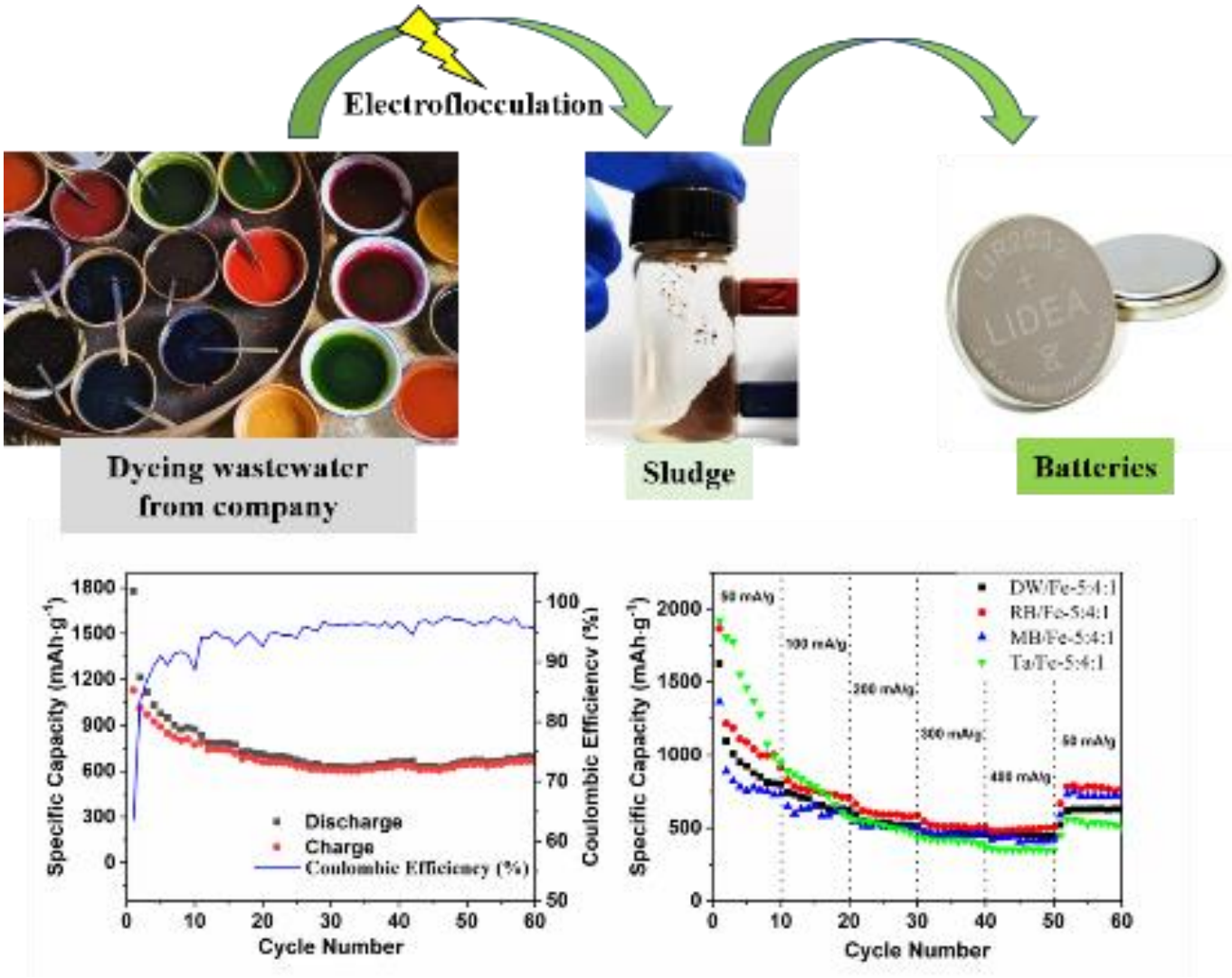

A series of sludges were produced by using a simple electroflocculation method to deal with the printing and dyeing wastewater from company. The sludges can be directly and effectively made into the anode electrodes of Li-ion battery. And the performance of electrodes can be improved by adding different proportions of super P® conductive carbon black. This idea not only helps companies save a lot of costs for waste treatment, but also provides a possibility to apply the treatment products in the distributed energy storage device.